Packing Stress Relaxation in Polymer–Lipid Monolayers at the Air–Water Interface: An X-ray Grazing-Incidence Diffraction and Reflectivity Study

ARTICLE *in* JOURNAL OF THE AMERICAN CHEMICAL SOCIETY · AUGUST 1999

Impact Factor: 12.11 · DOI: 10.1021/ja991048j

9 AUTHORS, INCLUDING:

Tonya L Kuhl
University of California, Davis
80 PUBLICATIONS **1,975** CITATIONS
SEE PROFILE

Jaroslaw Majewski
University of California, Davis
196 PUBLICATIONS **3,079** CITATIONS
SEE PROFILE

Ka Yee C. Lee
University of Chicago
156 PUBLICATIONS **3,885** CITATIONS
SEE PROFILE

Gregory Scott Smith
Oak Ridge National Laboratory
126 PUBLICATIONS **3,418** CITATIONS
SEE PROFILE

Packing Stress Relaxation in Polymer−Lipid Monolayers at the Air−Water Interface: An X-ray Grazing-Incidence Diffraction and Reflectivity Study

T. L. Kuhl,[‡] J. Majewski,[||] P. B. Howes,[§] K. Kjaer,[§] A. von Nahmen,[‡] K. Y. C. Lee,[⊥] B. Ocko,[#] J. N. Israelachvili,[‡] and G. S. Smith*,[||]

Contribution from the Materials Research Laboratory, University of California, Santa Barbara, California 93106, Manuel Lujan Jr. Neutron Scattering Center, Los Alamos National Laboratory, Los Alamos, New Mexico 87545, Department of Solid State Physics, Risø National Laboratory, DK-4000 Roskilde, Denmark, Department of Physics, Brookhaven National Laboratory, Upton, New York 11973, and Department of Chemistry, The University of Chicago, Chicago, Illinois 60637

Received April 1, 1999

Abstract: Using synchrotron grazing-incidence X-ray diffraction (GIXD) and reflectivity (XR), we have determined the in-plane and out-of-plane structure of phospholipid monolayers at the air−water interface as a function of hydrophilic lipid headgroup size. Di-stearoyl-phosphatidyl-ethanolamine (DSPE) lipid monolayers were systematically modified by chemically grafting hydrophilic poly(ethylene glycol) (PEG) chains of MW = 90 g/mol (2 ethylene oxide, EO, units), MW = 350 g/mol (8 EO units), and MW = 750 g/mol (17 EO units) to the lipid headgroups. The monolayers were studied in the solid phase at a surface pressure of 42 mN/m. At these high lipid packing densities, the PEG chains are submerged in the water subphase. The increased packing stresses from these bulky polymer headgroups distort the unit cell and the in-plane packing modes of the monolayers, leading to large out-of-plane alterations and staggering of the lipid molecules. Surprisingly, a change in the molecular packing of the monolayer toward *higher* packing densities (lower area per molecule) was observed on increasing the PEG MW to 750 g/mol (17 EO units). This rearrangement of the monolayer structure may be due to a conformational change in the PEG chains.

Introduction

The interactions between lipid bilayers and other flexible membranes, particularly at small separations, are governed by the interplay between direct molecular forces and entropic forces arising from fluctuations.[1−3] Recently, the stability and hydration of liposomes and surfaces bearing chemically grafted poly(ethylene glycol) (PEG) chains have been the focus of much interest due to their use as novel drug delivery vehicles and biologically passivating coatings.[4−9] The structure and surface properties of lipid assemblies before and after modification by the incorporation of PEG lipids with their bulky, hydrophilic headgroups are of considerable importance for predicting monolayer, bilayer, and liposome stability in such applications.[10−13]

Previously, we have investigated the structure of mixed polymer−lipid monolayers consisting of di-steroyl-phosphatidyl-ethanolamine (DSPE) and DSPE with chemically grafted poly(ethylene glycol) chains of MW = 2000 g/mol (DSPE-PEG_{2000}).[14,15] Mixtures of these lipids were stable at concentrations up to 10 mol % DSPE-PEG_{2000} and amenable to structural characterization using X-ray grazing-incidence diffraction and neutron and X-ray reflectivity. These studies indicated that bulky hydrophilic moieties caused significant out-of-plane protrusions of solid-phase phospholipid monolayers and presumably also of bilayers, vesicles, and biological membranes. In particular, our results suggested that the in-plane or lateral packing stresses due to the inclusion of bulky hydrophilic polymer−lipid headgroups of DSPE-PEG_{2000} within the monolayer were relaxed through an increase in out-of-plane protrusions and *not* by an increase in the area occupied per lipid molecule.

In our current work, we have probed much lower polymer molecular weights from PEG_{750} (17 EO monomers) to PEG_{90}

* To whom correspondence should be addressed.
[‡] University of California.
[||] Los Alamos National Laboratory.
[§] Risø National Laboratory.
[⊥] The University of Chicago.
[#] Brookhaven National Laboratory.

(1) Israelachvili, J. N. *Intermolecular and Surface Forces*; Academic Press: New York, 1992; p 450.
(2) Leikin, S.; Parsegian, V. A.; Rau, D. C. *Annu. Rev. Phys. Chem.* **1993**, *44*, 369−395.
(3) . Israelachvili, J. N.; Wennerstrom, H. *J. Phys. Chem.* **1992**, *96*, 520−531.
(4) Tirosh, O.; Barenholz, Y.; Katzhendler, J.; Priev, A. *Biophys. J.* **1998**, *74*, 1371−1379.
(5) Lasic, D.; Martin, D., Eds. *Stealth Liposomes*; CRC Press: Boca Raton, 1995; p 289 for a complete review.
(6) Harder, P.; Grunze, M.; Dahint, R.; Whitesides, G. M.; Laibinis, P. E. *J. Phys. Chem. B* **1998**, *102*, 426−436.
(7) Pertsin, A. J.; Grunze, M.; Garbuzova, I. A. *J. Phys. Chem. B* **1998**, *102*, 4918−4926.
(8) Sheth, S. R.; Leckband, D. *Proc. Natl. Acad. Sci. U.S.A.* **1997**, *94*, 8399−8404.
(9) Halperin, A. *Euro. Phys. J. B* **1998**, *3*, 359−364.
(10) Kenworthy, A. K.; Simon, S. A.; McIntosh, T. J. *Biophys. J.* **1995**, *68*, 1903−1920.
(11) Kenworthy, A. K.; Hristova, K.; Needham, D.; McIntosh, T. J. *Biophys. J.* **1995**, *68*, 1921−1936.
(12) Joannic, R.; Auvaray, L.; Lasic, D. D. *Phys. Rev. Lett.* **1997**, *78*, 3402−3405.
(13) Szleifer, I.; Gerasimov, O. V.; Thompson, D. H. *Proc. Natl. Acad. Sci. U.S.A.* **1998**, *95*, 1032−1037.
(14) Majewski, J.; Kuhl, T. L.; Kjaer, K.; Gerstenberg, M. C.; Als-Nielsen, J.; Israelachvili, J. N.; Smith, G. S. *J. Am. Chem. Soc.* **1968**, *90*, 1469−1473.
(15) Majewski, J.; Kuhl, T. L.; Gerstenberg, M. C.; Israelachvili, J. N.; Smith, G. S. *J. Phys. Chem B* **1997**, *101*, 3122−3129.

10.1021/ja991048j CCC: $18.00
Published on Web 08/06/1999

(2 monomers). We have focused on low molecular weight polymer−lipids because stable monolayers can be formed with the pure components and thus the complexities of a mixed system can be avoided. Hence, there is no longer any ambiguity concerning possible phase separation and it is generally simpler to model and extract structural information from single-component systems. Our current studies again point to the importance of out-of-plane fluctuations but also indicate that new modes of packing and lateral stress reduction are in play. In particular, we found that the molecules now tilt and distort the unit cell to increase the area per molecule for PEG_{90} and PEG_{350}. In contrast, a change in the molecular packing of the monolayer toward higher packing densities was observed upon increasing the PEG MW from 350 (8 EO units) to 750 g/mol (17 EO units). This rearrangement of the monolayer structure may be due to a conformational change in the PEG chains with increasing length.

Experimental Methods

In general, Langmuir monolayers are composed of 2D crystallites which are azimuthally randomly oriented on the water surface and therefore may be described as 2D powders. The reciprocal space GIXD patterns from the 2D ordered-crystalline monolayers on the liquid surface arise from a 2D array of *Bragg rods*,[16,17] which extend parallel to the vertical scattering vector q_z.[18] The scattered intensity was measured by scanning over a range of the horizontal scattering vector, $q_{xy} \approx (4\pi/\lambda)\ \sin(2\theta_{xy}/2)$, where $2\theta_{xy}$ is the angle between the incident and diffracted beam projected onto the horizontal plane, and λ is the wavelength of the X-ray beam. Such a scan, integrated over the whole window of a position-sensitive detector (PSD), yields the *Bragg peaks*. Simultaneously, the scattered intensity recorded in channels along the PSD, but integrated over the scattering vector in the horizontal plane across a Bragg peak, produces q_z-resolved scans called *Bragg rod profiles*. The intensity distribution along a Bragg rod can be analyzed to obtain information on the direction and magnitude of the molecular tilt in the crystalline part of the amphiphilic film (we assumed a cylindrical electron distribution for the tails), the length, L_c, of the part of the molecule which scatters coherently, and the magnitude of molecular motion or surface roughness of the crystallites (Debye−Waller factor).[16,17] In addition, detailed information on the electron density distribution in the vertical direction, laterally averaged over both the ordered and disordered parts of the film, can be obtained from the deviation of the measured specular X-ray reflectivity from Fresnel's law.[16,17]

The reflectivity data were analyzed using a kinematic approach.[16,17] The monolayer electron density distribution was approximated by boxes of various lengths and electron densities, which correspond to the structural components of the layer, e.g., hydrocarbon tails, lipid headgroups, and PEG chains. Our philosophy was to use the simplest physically reasonable model to fit the experimental data. We began with a two-box model to describe DSPE, one box for the tail region and another for the headgroup. A single Gaussian roughness was used to smear the interfaces and the resulting model reflectivity was compared to the data. The DSPE-PEG_{MW} (DSPE, DSPE-PEG_{90}, PEG_{350}, and PEG_{750}) monolayers were initially modeled with two boxes also, one for the DSPE tail section and another for the DSPE headgroup−PEG polymer chains. We then systematically increased the complexity of our model by adding additional boxes, until χ^2 was minimized and no longer significantly decreased upon increasing the number of fitting parameters. This procedure ensured that the problem was not over-parametrized. We found that in the most complicated case 6 boxes were needed to obtain a reasonable fit to the entire reflectivity profile. We did not find a significant improvement in the fits to the reflectivity data when an exponential or parabolic form was used to model the polymer layer.[19−21] This is most likely due to the short length of the polymer chains used in this study. For this reason, the polymer layer was modeled as a simple step function.[22,23]

By combining the methods of grazing-incidence X-ray diffraction and X-ray specular reflectivity, the in-plane and out-of-plane structure of thin amphiphilic films at air−liquid interfaces can be well characterized. We performed the GIXD and reflectivity experiments at the BW1 (undulator) beam line at the HASYLAB synchrotron source (Hamburg, Germany)[24] and on the Harvard/Brookhaven National Laboratory bending magnet ×22B line at the National Synchrotron Light Source (X-ray reflectivities)[25] using liquid surface diffractometers. The amphiphilic monolayers were spread on a Millipore filtered water subphase from 5×10^{-6} M 1:9 methanol−chloroform solutions. All lipids were obtained from Avanti Polar Lipids. The trough was equipped with a Wilhelmy balance and a barrier for surface pressure control and thermostated to 21 °C. After spreading a film, the trough container was flushed with helium to reduce the scattering background and to minimize beam damage during the scans. As an additional precaution, the trough was moved by 0.025 mm in the horizontal plane, perpendicular to the incident beam, for each step during the $2\theta_{xy}$ scans. Typical scans lasted 1 to 2 h.

The pressure−area isotherms for the four different DSPE-PEG_{MW} lipids are shown in Figure 1. As can be seen, the PEG portion of the lipid headgroup is also surface active,[14,15] and a non-zero surface pressure is detected even at very large areas per molecule. However, as the molecules are compressed, the DSPE-PEG_{MW} isotherms become almost superimposed, approaching that of unmodified DSPE, indicating that the PEG portion of the molecules is pushed down into the water subphase. No indication of domain formation or structuring within the monolayer at the air−water interface was observed using fluorescence or Brewster angle microscopy (results not shown). To investigate how the size of the PEG headgroup affects the physical structure and packing within the monolayers, GIXD and reflectivity measurements were conducted on these three DSPE-PEG_{MW} monolayers at a surface pressure of 42 mN/m.

Results

Grazing-Incidence X-ray Diffraction. The GIXD provided information on the crystalline portions of the monolayers. For diacyl phospholipid monolayers at the air−water interface, diffraction is observed from the lateral order of the tails only.[26] Figure 2 shows low-order diffraction data for DSPE and DSPE-

(16) Als-Nielsen, J.; Kjaer, K. X-ray Reflectivity and Diffraction Studies of Liquid Surfaces and Surfactant Monolayers. In *The Proceedings of the NATO Advanced Study Institute, Phase Transitions in Soft Condensed Matter*; Geilo, Norway, April 4−14, 1989; Plenum Publishing Corp.: New York, 1989; pp 113−137.

(17) Kjaer, K. *Physica B* **1994**, *198*, 100. Proceedings of the 3rd International Conference on Surface X-ray and Neutron Scattering, Dubna, Russia, June 24−29, 1993.

(18) To maximize surface sensitivity for the GIXD measurements the monochromatic X-ray beam was adjusted to strike the surface at an incident angle ≈0.11°, which corresponds to a momentum transfer vector of $q_z \approx 0.85q_c$, where $q_c = 0.02176$ Å^{-1} is the critical scattering vector for total external reflection. See, for example, Eisenberger, P.; Marra, W. C. *Phys. Rev. Lett.* **1981**, *46*, 1081. The dimensions of the footprint of the incoming X-ray beam on the liquid surface were approximately 5×50 mm^2. For the collection of the diffracted intensities we used a one-dimensional position-sensitive detector (PSD) with vertical acceptance $0 < q_z < 0.9$ Å^{-1}, and its axis along the vertical. In front of the PSD a Soller collimator was mounted which defined the horizontal resolution of the detector, $\Delta q_{xy} = 0.0075$ Å^{-1}.

(19) Milner, S.; Witten, T.; Cates, M. *Macromolecules* **1988**, *21*, 2610−2618.

(20) Szleifer, I.; Carignano, M. A. Tethered Polymer Layers. In *Advances in Chemical Physics*; Prigogine, I., Rice, S. A., Eds.; Wiley: New York, 1996; pp 165−259.

(21) Kent, M. S.; Lee, L. T.; Factor, B. J.; Rondelez, F.; Smith, G. S. *J. Chem. Phys.* **1995**, *103*, 2320−2342.

(22) Alexsander, S. *J. Phys. Paris* **1977**, *38*, 983−987.

(23) de Gennes, P. G. *Macromolecules* **1980**, *13*, 1069−1075.

(24) Majewski, J.; Popovitz-Biro, R.; Bouwman, W. G.; Kjaer, K.; Als-Nielsen, J.; Lahav, M.; Leiserowitz, L. *Chem. Eur. J.* **1995**, *1*, 304. Weissbuch, I.; Popovitz-Biro, R.; Lahav, M.; Leiserowitz, L.; Kjaer, K.; Als-Nielsen, J. *Isr. Adv. Chem. Phys.* **1997**, *102*, 39−120.

(25) Braslau, A.; Pershan, P. S.; Swislow, G.; Ocko, B. M.; Als-Nielsen, J. *Phys. Rev. A* **1988**, *38*, 2457.

(26) Kjaer, K.; Als-Nielsen, J.; Helm, C. A.; Laxhuber, L. A.; Möhwald, H. *Phys. Rev. Lett.* **1987**, *58* (21), 2224. Boehm, C.; Möhwald, H.; Leiserowitz, L.; Als-Nielsen, J.; Kjaer, K. *Biophys. J.* **1993**, *64* (2), 553−9.

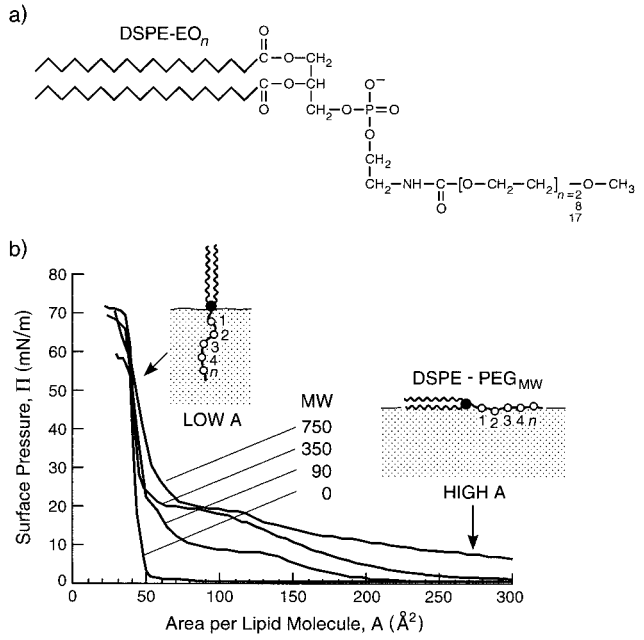

Figure 1. (a) Chemical structure of DSPE-EO$_n$. (b) Monolayer compression (Π-A) isotherms of (a) pure DSPE, (b) DSPE-PEG$_{90}$, (c) DSPE-PEG$_{350}$, and (d) DSPE-PEG$_{750}$ at 21 °C. The area, *A*, is the mean area per molecule at the air−water interface. At high surface pressures (Π > 30 mN/m) the lateral interactions of the polymer chains are not evident in the pressure isotherm, as the polymer chains are completely submerged in the water subphase. Inset: Schematic configuration of DSPE-EO$_n$ at the air−water interface at high and low areas.

PEG$_{MW}$ with both q_{xy} and q_z resolved. For pure DSPE monolayers the {1,0} reflection and higher order hexagonal reflections {1,1} and {2,0} were observed.[27] By contrast, only the {1,0} reflection was observable for the DSPE-PEG$_{MW}$ monolayers. Figure 3 shows the data projected on the q_{xy} axis, yielding Bragg peaks, and intensities integrated over the Bragg peaks, as a function of q_z (the Bragg rods), are shown in Figure 4. Clearly, for unmodified DSPE the peak is not split, indicating a hexagonal lattice of the chains. The Bragg rod exhibits one broad maximum, located at $q_z \approx 0$[28] (Figures 2 and 4). This indicates that the chains have little tilt in the pure DSPE monolayer. Attaching two EO monomers (PEG$_{90}$) to the DSPE headgroup induces a tilt of the chains, two maxima in the q_z direction being now evident (Figures 2 and 4). However, the PEG$_{90}$ *lattice* is still predominantly hexagonal, as these two peaks are at almost the same q_{xy} value. The ratio of the peak intensities is approximately 1:2 and the positions of their intensity maxima ($q_z \approx 0$ and $q_z > 0$) indicate[16,17] that the molecules tilt approximately toward their nearest neighbor.[29] The packing structure of the lipid monolayer changes further as the number of EO units increases to 8 for PEG$_{350}$. Again, two maxima in the intensity of the Bragg rods are evident (Figures 2 and 4), but they occur at two clearly separate q_{xy} positions indicating a distortion of the hexagonal cell.[30] The ratio of the intensities

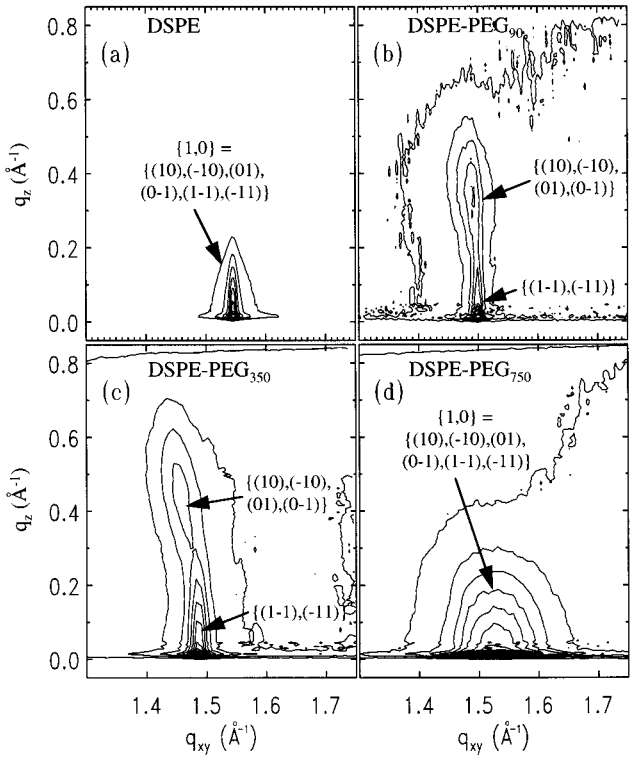

Figure 2. Grazing-incidence X-ray diffraction measurements from (a) pure DSPE, (b) DSPE-PEG$_{90}$, (c) DSPE-PEG$_{350}$, and (d) DSPE-PEG$_{750}$ monolayers at 42 mN/m at 21 °C. The two-dimensional contour plots of the intensity distribution $I(q_{xy},q_z)$ along the horizontal (q_{xy}) and the vertical (q_z) scattering vectors are shown. The number of observed peaks and their position in (q_{xy},q_z) space indicate different unit cells and angle of molecular tilt.

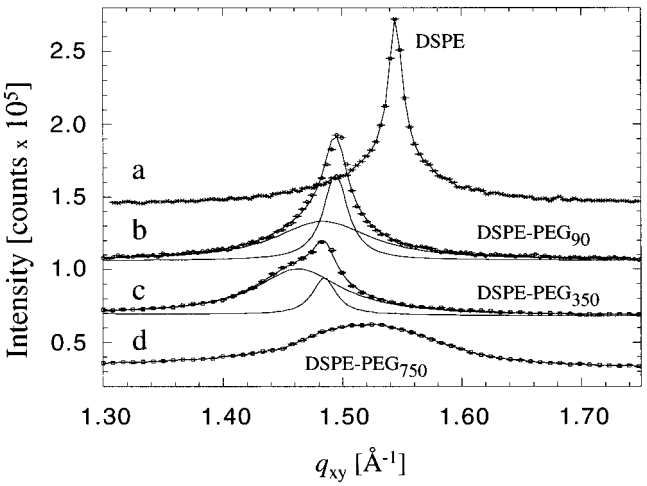

Figure 3. Grazing-incidence X-ray diffraction data at a surface pressure of 42 mN/m for (a) pure DSPE, (b) DSPE-PEG$_{90}$, (c) DSPE-PEG$_{350}$, and (d) DSPE-PEG$_{750}$. The Bragg peak profiles were obtained by scanning along the horizontal scattering vector q_{xy} ($q_{xy} \approx (4\pi/\lambda)\sin(2\theta_{xy}/2)$), where $2\theta_{xy}$ is the horizontal angle between the incident and diffracted beam and λ is the wavelength of the X-ray beam and integrating over the whole q_z window of the position sensitive detector. For the DSPE-PEG$_{90}$ and DSPE-PEG$_{350}$ monolayers, the Bragg peaks are not symmetric, indicating a small distortion of the hexagonal lattice. These peaks (solid lines) were deconvoluted into two Bragg reflections using a least-squares fitting procedure. The parameters of the distorted hexagonal unit cell and coherence lengths for the reciprocal lattice vectors are listed in Table 1.

and their positions at $q_z \approx 0$ and $q_z > 0$ once again indicates that the molecules are tilted toward their nearest neighbors.[16,17]

(27) {*hk*} denotes a set of Bragg rods (*hk*) with equal in-plane components $|\vec{q}_{xy}^{hk}|$, hence not resolved in GIXD from these 2D powders. E.g., for the hexagonal lattice {10} means {(10),(01),(10),(0$\bar{1}$),(11),(1$\bar{1}$)}.

(28) The sharp peak at $q_z = 0.01$ Å^{-1} is the so-called Vineyard−Yoneda, which arises from the interference between X-rays diffracted up into the Bragg rod and rays diffracted down and then reflected up by the interface, cf.: Vineyard, G. *Phys. Rev. B* **1982**, *26*, 4146.

(29) To obtain a good fit to the Bragg rod data for PEG$_{90}$, a deviation from the nearest neighbor direction of the tilt azimuth by 10° had to be assumed.

(30) The distorted lattice, with $a = b$, $\gamma \neq 120°$, can also be described as a {centered} rectangular lattice: a_r, $b_r \neq \sqrt{3}a_r$, $\gamma_r = 90°$.

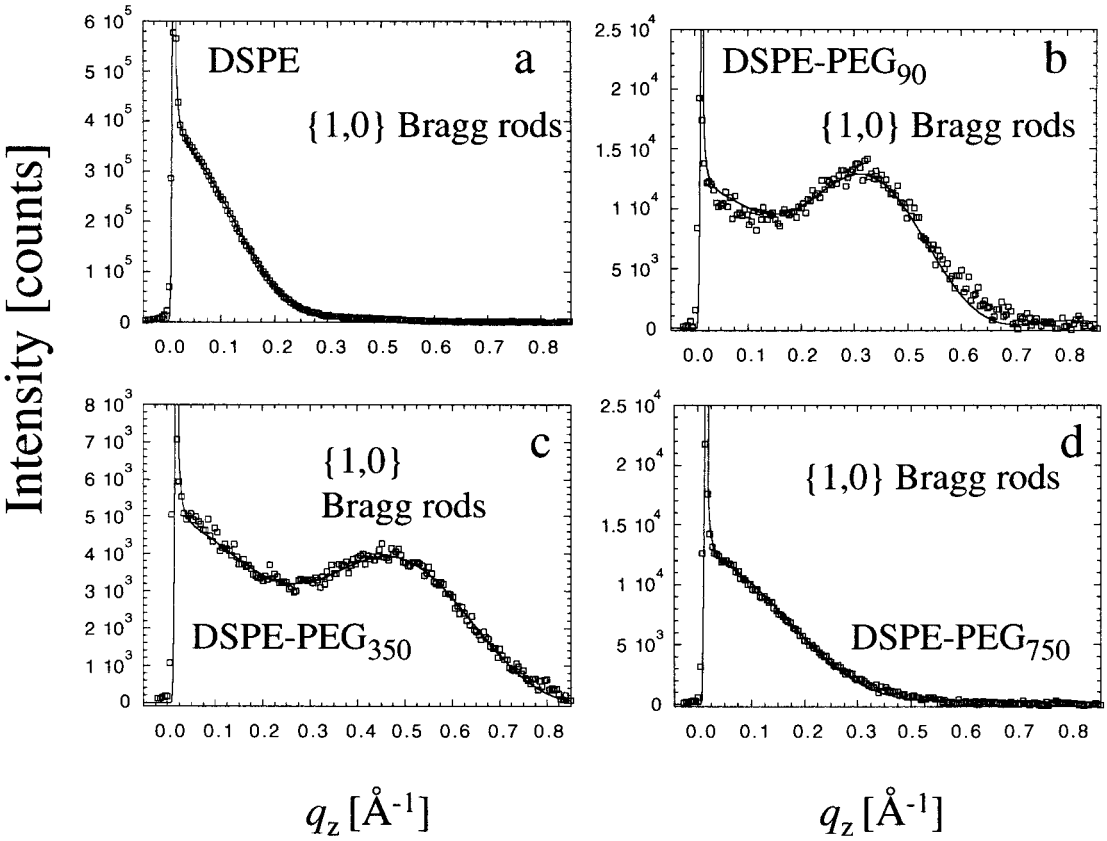

Figure 4. Bragg rods: scattered intensity distribution perpendicular to the water surface and integrated (after background subtraction) over the q_{xy} range of each Bragg peak to yield Bragg rods: (a) pure DSPE, (b) DSPE-PEG_{90}, (c) DSPE-PEG_{350}, and (d) DSPE-PEG_{750}. The rods were fitted (solid line) by approximating the coherently scattering part of the phospholipid tail by a cylinder of a constant electron density. The molecular packing parameters used in the fitting procedure are listed in Table 1. All samples were compressed to a surface pressure of 42 mN/m.

Table 1. Results, Both In-Plane and Out-of-Plane, from Fitting the GIXD Diffraction Peaks Shown in Figures 3 and 4

	in−plane Bragg peaks							out-of-plane Bragg rods			
compo-sition	obsd *d* spacing (Å)	area per molecule (Å^2)	projctd area (Å^2)	primitive unit cell *a*, *b*, *γ* (Å, Å, deg)			coherence length, *L* (Å)	coherence length, L_c (Å)	tilt angle, *t* (deg)	tilt dir (deg)	σ_z (Å)
DSPE	$d_{10} = d_{01} = d_{1-1} = 4.07$	38.3	38.2	4.70	4.70	120.0	$L_{10,01,1-1} = 360$	23.5	3.8	n/a[b]	0.5
PEG_{90}[a]	$d_{10} = d_{01} = 4.21$ $d_{1-1} = 4.19$	40.8	39.4	4.85	4.85	119.7	$L_{10,01} = 58$ $L_{1-1} = 240$	21.0	15.3	NN ± 10	0.4
PEG_{350}[b]	$d_{10} = d_{01} = 4.31$ $d_{1-1} = 4.23$	42.4	39.7	4.91	4.91	118.6	$L_{10,01} = 63$ $L_{1-1} = 250$	15.6	20.3	NN	0.9
PEG_{750}	$d_{10} = d_{01} = d_{1-1} = 4.11$	39.0	38.8	4.74	4.74	120.0	$L_{10,01,1-1} = 41$	16.0	5.0	n/a[b]	0.5

[a] The distorted-hexagonal lattice, with $a = b$, $\gamma \neq 120°$, can be described as a centered rectangular one: $a_r = \boldsymbol{a} + \boldsymbol{b}$, $b_r = \boldsymbol{a} - \boldsymbol{b} \neq a_r\sqrt{3}$, $\gamma_r = 90°$. [b] The tilt direction is not well-determined for small tilt angle.

Upon further increasing the number of EO units to 17, PEG_{750}, the packing within the monolayer changes back to hexagonal and only one broad peak at $q_z \approx 0$ is present, indicating that the molecules are not tilted and stand perpendicular to the interface, Figures 2 and 4.

Table 1 summarizes the results, both in-plane and out-of-plane, from fitting the GIXD diffraction peaks shown in Figures 3 and 4. Quantitatively, using the Scherrer formula,[31] we find that the in-plane crystallite domain size is 360 Å for pure DSPE and decreases to 58 and 240 Å for PEG_{90}, 63 and 250 Å for PEG_{350}, and a mere 41 Å for PEG_{750}. The unit cell dimensions were obtained by fitting the peak positions. For the in-plane symmetrical peaks, DSPE and PEG_{750}, one peak was used, while the large asymmetry for PEG_{90} and PEG_{350} required two peaks. The out-of-plane coherence length L_c was obtained by fitting the integrated Bragg rod intensities, as shown in Figure 4. The coherently scattering portion of the lipid tails for unmodified DSPE corresponds to a fully stretched C_{18} chain, $L_c = 23.5$ Å, Table 1 (out-of-plane). The coherence length decreases from 23.5 to 21.0 and 15.6 Å as the number of EO monomers in the headgroup increases from 0 to 2 and 8. Similarly, the unit cell becomes more distorted from hexagonal packing with little tilt for DSPE to tilted in a slightly distorted lattice for PEG_{90} and to tilted molecules in a more distorted lattice for PEG_{350}, respectively. However, this trend of increasing distortion of the unit cell does not continue. At 17 EO units for PEG_{750}, no further reduction in the out-of-plane coherence length occurs, $L_c = 16.0$ Å. Moreover, the in-plane diffraction indicates that the structure returns to hexagonal packing and the molecules once again stand almost perpendicular to the air−water interface with a corresponding decrease in the *d* spacing. In other words, the unit cell and the packing of the molecules almost return to that of unmodified DSPE, but at the expense of a reduced out-of-plane coherence length (16.0 vs 23.5 Å) and size of the scattering islands (360 vs 41 Å).

(31) Guinier, A. *X-ray Diffraction*; Freeman: San Francisco, 1968; eq 5.3. The in-plane coherence length is the average distance, in the direction of the reciprocal lattice vector $\boldsymbol{q}_{xy}$, over which "near-perfect" crystallinity extends in the 2-D crystallites.

Table 2. Electron Density and Thickness Data

composition	tail region thickness (Å)		tail region electron density,[a,b] ρ		tail region total thickness L_t[b] (Å)	headgroup region thickness (Å)		headgroup region electron density,[a,b] ρ		headgroup region total thickness L_h[b] (Å)	polymer region thickness (Å)		polymer region electron density,[a,b] ρ		polymer region total thickness L_p[b] (Å)	σ (Å)	χ^2
DSPE	21.13		0.971 (274)		21.13 (274)	9.04		1.426 (172)		9.04						3.42	17.6
PEG_{90}	10.34	10.22	0.968 (134)	1.005 (137)	20.56 (271)	9.57		1.469 (188)		9.57 (188)	4.42		1.104 (65)		4.42 (65)	3.37	4.14
PEG_{350}	10.10	10.61	0.798 (108)	1.019 (144)	20.71 (252)	7.52	12.30	1.480 (149)	1.179 (194)	17.59 (343)	11.50	25.40	1.043 (160)	1.002 (340)	11.50+ (500)	3.80	3.45
PEG_{750}	6.98	14.53	0.771 (72)	1.043 (203)	21.51 (275)	11.11	9.34	1.244 (185)	1.114 (139)	20.45 (324)	14.46	11.98	1.067 (206)	1.024 (164)	26.44 (370)	3.72	3.02

[a] All electron denisties are normalized by the electron density of water, $\rho_{water} = 0.334\ e^-/Å^3$.The area per molecule was kept 40 Å^2 for the model fitting. σ is the root-mean-square roughness of the interface. [b] The number of electrons is given in parentheses.

Reflectivity. In contrast to the GIXD measurements, reflectivity provides information on both the 2D-crystalline and amorphous parts of the monolayer. The reflectivity data were analyzed using the kinematical approach and the electron density profiles were approximated with boxes of various thicknesses and electron densities.[16,17] The unmodified DSPE monolayer could be modeled with two boxes (see Table 2, Figure 5): one box for the headgroup region, 9.04 Å long, and with normalized electron density 1.426 (all electron densities are reported normalized to that of the water subphase, 0.334 $e^-/Å^3$) and one box of length 21.3 Å and electron density 0.971 for the tail, in agreement with previous studies.[32] To obtain a good fit to the DSPE-PEG_{90} reflectivity profiles, we added a box to account for the polymer layer, but also found it necessary to divide the tail region of the phospholipid into two parts, one with higher electron density located next to the headgroup region and one with lower electron density in contact with air. The total number of electrons within these two boxes was still close to the theoretical electron density of two C_{18} chains. We found it necessary to further divide the headgroup into two boxes as the number of EO monomers increased from 2 to 17 EO units. Parameters obtained from this fitting procedure are summarized in Table 2 and Figure 5. The fitting scheme and necessity of dividing the tail region into two sections, one with higher and one with lower electron density, is demonstrated in Figure 6. Only when this was done were the reflectivity profiles well reproduced by the models.

In all cases, the tail region of the lipid layer is 21 ± 0.5 Å thick; however, the electron density distributed between the two boxes composing this layer changes with increasing number of EO units. By modeling the tail region with two boxes, we see that the box representing the tail region adjacent to the lipid headgroups has an electron density slightly greater than that for close-packed hydrocarbon chains, while the box against air has a lower than expected electron density. Likewise, the boxes used to model the headgroup region have a systematically decreasing electron density (closer to water) but increasing thickness as compared to unmodified DSPE. Indeed, the thickness of the headgroup region doubles from 9 to 20 Å for PEG_{750}. As we will discuss in the next section, these results imply a mixing and contribution of different parts of the molecule in each of the boxes, i.e., a mixing of polymer with the lipid headgroup region, headgroup with tail, and participation of air in the tail region. These changes are most likely due to staggering of molecules and structural rearrangements. Finally, the thickness of the polymer layer increases with increasing number of EO units. The weak contrast between PEG and water makes it difficult to quantify the extent and density of this layer.[33] However, as shown in Figure 5 a region of higher scattering density as compared to water slowly decays from the headgroup region into the water subphase. Finally, there is only a moderate increase in the root-mean-square roughness σ of the monolayer as the number of EO units increases.[34]

Discussion and Conclusions

As regards the in-plane packing, our results indicate that in the series DSPE, PEG_{90}, to PEG_{350} the unit cell size increases. As the number of ethylene oxide monomers increases, the area per lipid molecule increases which increases the tilt, thereby reducing the lateral packing stresses. By contrast, with PEG_{750} there was a change in the monolayer packing properties. The unit cell shrank and the molecules returned to a perpendicular packing relative to the air−water interface. However, this was at the expense of in-plane correlation length. The average coherence length in the 2D crystallites was reduced to 41 Å corresponding to coherently scattering clusters of only about 43 lipid molecules. This decrease in crystalline domain size (coherence lengths, *L*, see Table 1) as a function of PEG chain length is due to lateral PEG-PEG interactions as well as PEG−lipid headgroup interactions, i.e., osmotic pressure, configurational entropy, water solvation, etc., which act to disrupt the in-plane packing order within the monolayer.

Similar trends were seen in the out-of-plane scattering. The coherently scattering part of the molecules decreased from a fully stretched C_{18} chain for DSPE (23.5 Å) to a low of about 16 Å for the DSPE-PEG_{750} lipids. This suggests that the lipid molecules stagger to reduce the repulsive PEG modified headgroup−headgroup interactions. We see this staggering by reflectivity as well. Both the tail and headgroup regions must be divided into higher and lower scattering density boxes. A plausible model of this structure is depicted in Figure 7. By combining the structural data obtained from the GIXD and reflectivity measurements, we estimate the maximum staggering or lipid−lipid off-set to be about 10 Å, e.g., the coherence length decreases from 23.5 to 15.6 Å. Likewise, good fits were obtained to the reflectivity data only when the head and tail regions were divided into 10 Å regions of differing electron density. This 10 Å of staggering also corresponds to the size of an unmodified DSPE headgroup. These results taken together with the distortions in the unit cell and different packing modes from tilted hexagonal to tilted rectangular and back to nontilted hexagonal for PEG_{90}, PEG_{350}, and PEG_{750}, respectively, suggest that the lateral PEG modified headgroup−headgroup repulsion was

(32) Helm, C. A.; Tippman-Drayer, P.; Mohwald, H.; Als-Nielsen, J.; Kjaer, K. *Biophys. J.* **1991**, *60*, 1457. Helm, C. A.; Mohwald, H.; Als-Nielsen, J.; Kjaer, K. *Biophys. J.* **1987**, *52*, 381.

(33) The electron density of bulk PEG is only 6% higher than the water subphase.

(34) We were surprised that the monolayer roughness, σ, was not significantly increased by molecular staggering. It may be that the gauche defects and disorder, as sketched in Figure 7, cause the air−monolayer interface to have a relatively smooth appearance.

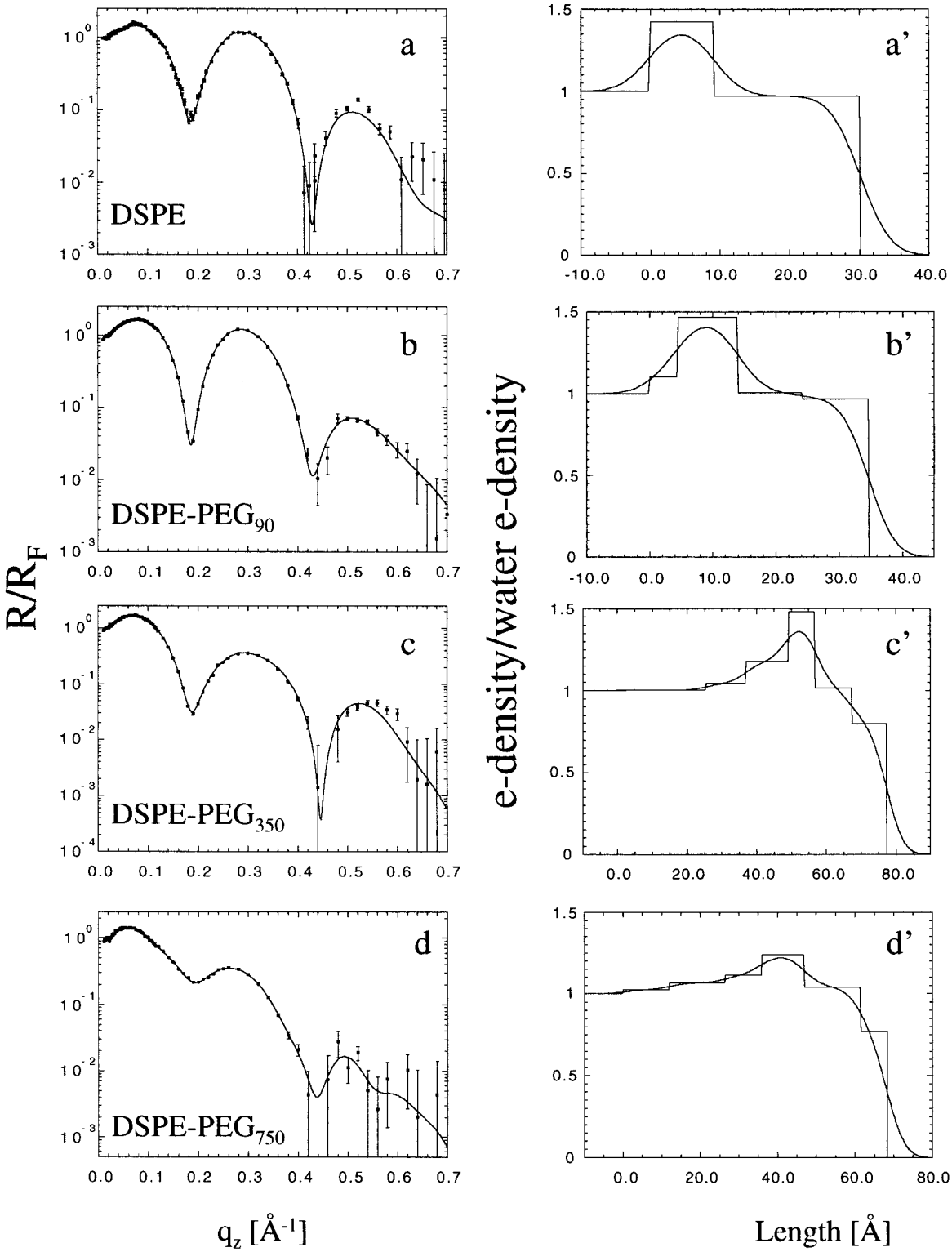

Figure 5. X-ray reflectivity data at a surface pressure of 42 mN/m for (a) pure DSPE, (b) DSPE-PEG$_{90}$, (c) DSPE-PEG$_{350}$, and (d) DSPE-PEG$_{750}$; the solid lines are fits to the data using box models discussed in the text. (a′, b′, c′, d′) The corresponding electron density profiles obtained from the fittings (parameters shown in Table 2). The steplike profiles are the unsmeared electron density profile, while the smooth curves result when the box models are convoluted with the root-mean-square interfacial roughness σ. R/R_F is the measured reflectivity normalized by the Fresnel reflectivity, R_F, for an ideal, infinitely sharp air−water interface.

reduced through two different modes: one, by *increasing the area per molecule* and molecular tilt, which thereby reduces the headgroup−headgroup interaction, and two, by *staggering the headgroups* out of the monolayer plane.

It was surprising that the trend of greater unit cell distortion and reduced out-of-plane coherence length, L_c, did not continue as the number of EO monomers increased from 2 (PEG$_{90}$) and 8 (PEG$_{350}$) to 17 (PEG $_{750}$). One possible explanation for this behavior is a structural change induced or stabilized by increasing the number of EO monomers.[6,7] PEG can form hydrogen bonds both with itself and with water. PEG is known to form helical coils in the solid phase and to retain some of

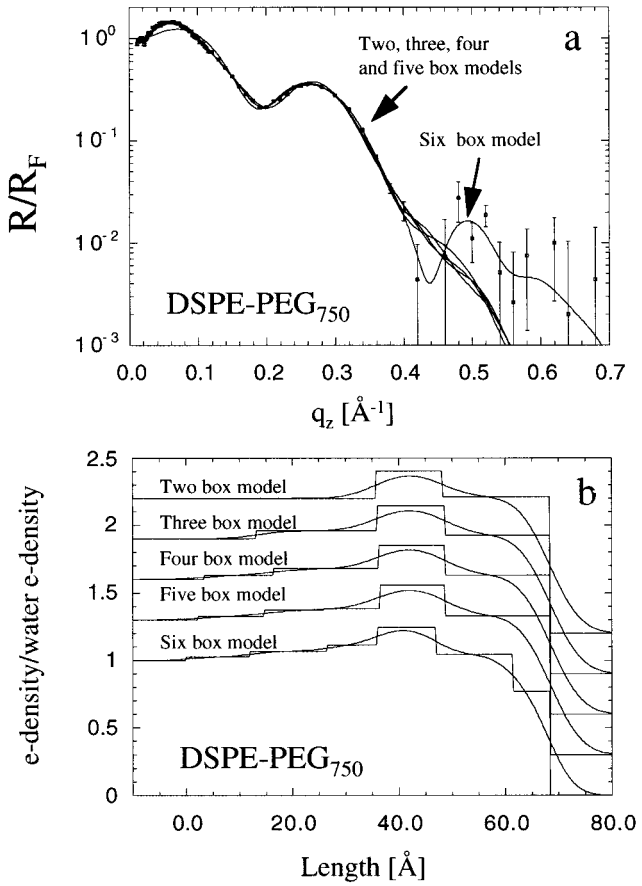

Figure 6. (a) X-ray reflectivity data for DSPE-PEG$_{750}$. The solid lines are fits to the data using multiple box models. (b) The corresponding smeared and unsmeared electron density profiles for two through six box models. The only model for which a reasonable fit is obtained to the entire reflectivity profile especially at higher momentum transfers occurs when the lipid tail region is divided into two boxes, one with lower electron density in contact with air and one with higher electron density located next to the headgroup region. The fitted electron densities were offset by 0.3 along the *y* axis.

this helical structure in water.[35−37] From X-ray diffraction measurements, the pitch of these helices in the solid phase is 19 Å and composed of 14 EO monomers.[38,39] Thus, if we have two such helices adjacent to each other as in a PEG$_{750}$ monolayer, another way of reducing the lateral headgroup−headgroup or rather PEG-PEG repulsion would be to offset these helices by half the pitch and so enable some interdigitation. Because half the helix pitch correlates well with the size of a lipid headgroup, it may be that interdigitation opens another pathway by which the lateral tension between adjacent molecules may be reduced. We do not suggest that this helix formation *alone* causes a change in the packing modes of the monolayer. However, this is another consideration whereby the energy of packing is minimized by offsetting the headgroup registry. The monolayer is highly disrupted as manifested by the small crystallite domain size of 41 Å, but the lateral repulsion would be reduced.

Last, in contrast to these studies, our previous work on *mixed* monolayers of DSPE with longer chained DSPE-PEG$_{2000}$ at concentrations up to 10 mol % indicated that the lateral stresses induced by larger polymeric headgroups did not distort the dimensions of the lipid unit cell. Instead, these monolayers reduced the packing stresses predominately through out-of-plane protrusions, similarly to DSPE-PEG$_{750}$ (Figure 7d).

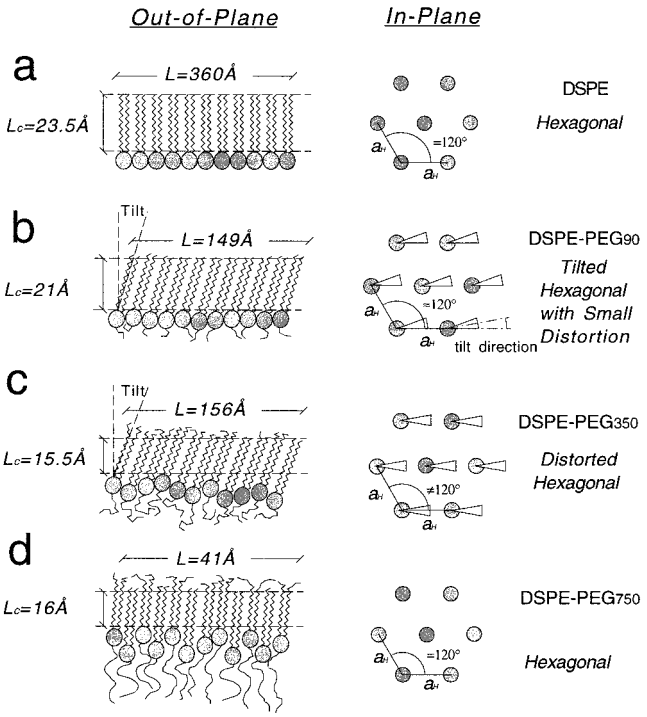

Figure 7. Schematic of how the out-of-plane and in-plane structure of the lipid monolayers changes with increasing EO monomer units. With increasing number of EO monomers the coherently scattering portion of the lipid tails, L_c, decreases from 23.5 Å, 21.0 Å, 15.6 Å, to 16.0 Å for DSPE, DSPE-PEG$_{90}$, DSPE-PEG$_{350}$, and DSPE-PEG$_{750}$, respectively. Evidently, the tail end (against air), as well as the tail part nearest to the lipid head, becomes more out of register and these portions of the hydrocarbon layer become more and more disordered as depicted schematically. As a result, the molecules obtain more space for lateral disorder, but no longer Bragg scatter so the out-of-plane coherence length decreases. Similarly, the unit cell becomes more tilted and distorted with increasing PEG MW. However, this trend does not continue as the number of monomers increases from 8 to 17. For chains greater than 14 monomers, it may be possible for PEG to form helices.[35,36] Interdigitation of neighboring helical chains would be another way of reducing the lateral PEG-PEG repulsion.

Acknowledgment. We gratefully acknowledge beamtime at HASYLAB at DESY, Hamburg, Germany, and funding by the programs DanSync (Denmark) and TMR-Contract ERBFM-GECT950059 of theEuropean Community. This work was supported (in part) under the auspices of the United States Department of Energy. The Manuel Lujan Jr., Neutron Scattering Center is a national user facility funded by the United States Department of Energy, Office of Basic Energy Sciences-Materials Science, under contract No. W-7405-ENG-36 with the University of California. Brookhaven National Laboratory is supported by the Division of Materials Research, U.S Department of Energy under contract DE-AC02-98CH10886. K.Y.C.L. is grateful for the support from the Camille and Henry Dreyfus New Faculty Award (NF-98-048). This work was partially supported by the MRL Program of the National Science Foundation under Award No. DMR-96-32716 and the MRSEC Program under Award No. DMR-9123048 with the University of Chicago. We are grateful to David Vaknin for the use of his trough.

JA991048J

(35) Koenig, J. L.; Angood, A. C. *J. Polym. Sci. A-2* **1970**, *8*, 1787−1796.
(36) Sandell, L. S.; Goring, D. A. I. *J. Polym. Sci. A-2* **1971**, *9*, 115−126.
(37) Miyazawa, T.; Fukushima, K.; Ideguchi, Y. *J. Chem. Phys.* **1963**, *37*, 2764−2776.
(38) Miyazawa, *J. Polym. Sci.* **1961**, *55*, 215.
(39) Koenig, J. L.; Angood, A. C. *J. Polym. Sci. A-2* **1970**, *8*, 1787−96.